OPTICA

Bell state analyzer for spectrally distinct photons

Navin B. Lingaraju,[1,2,†,*] Hsuan-Hao Lu,[1,†] Daniel E. Leaird,[1] Steven Estrella,[3] Joseph M. Lukens,[4] and Andrew M. Weiner[1]

[1]School of Electrical and Computer Engineering, Purdue University, West Lafayette, Indiana 47907, USA
[2]Advanced Technology and Systems Division, SRI International, Arlington, Virginia 22209, USA
[3]Freedom Photonics, LLC, 41 Aero Camino, Santa Barbara, California 93117, USA
[4]Quantum Information Science Section, Oak Ridge National Laboratory, Oak Ridge, Tennessee 37831, USA
*Corresponding author: navin.lingaraju@sri.com

Received 13 September 2021; revised 10 January 2022; accepted 24 January 2022; published 4 March 2022

We demonstrate a Bell state analyzer that operates directly on frequency mismatch. Based on electro-optic modulators and Fourier-transform pulse shapers, our quantum frequency processor design implements interleaved Hadamard gates in discrete frequency modes. Experimental tests on entangled-photon inputs reveal fidelities of ∼98% for discriminating between the $|\Psi^+\rangle$ and $|\Psi^-\rangle$ frequency-bin Bell states. Our approach resolves the tension between wavelength-multiplexed state transport and high-fidelity Bell state measurements, which typically require spectral indistinguishability. © 2022 Optical Society of America under the terms of the OSA Open Access Publishing Agreement

https://doi.org/10.1364/OPTICA.443302

Unlocking the potential of quantum technology will require not just progress in developing stand-alone systems but also in mediating communications and entanglement between these systems across a network [1]. Protocols have been devised to herald the generation of remote entanglement between previously unentangled parties, often through Bell state measurements [2–4]. In the simplest conception of such a protocol, two photons, each entangled with separate qubits (either matter-based or photonic), are mixed at a 50:50 spatial beam splitter. Quantum interference between two-photon outcomes leads to one of many detection events, a subset of which heralds projection of the undetected qubits onto a *known* entangled state. Similarly, in quantum teleportation [5–7], a Bell state measurement performed on an unknown input qubit and one half of an entangled pair projects the remaining qubit onto the state of the original input—up to a known unitary rotation—all without physical transmission of the quantum state itself.

However, a limitation of conventional Bell state measurements is that photons participating in the joint measurement need to be spectrally indistinguishable in order to project the remaining undetected particles onto a *known* entangled state. For the case when photons are separated by a frequency difference $\Delta\omega$ and detected a time Δt apart, the undetected qubits are projected onto an entangled state with an additional phase shift $e^{i\Delta\omega\Delta t}$ [8,9]. Irrespective of whether one applies temporal postselection or active feedforward techniques to compensate for this fluctuating term, the fidelity of remote entanglement is ultimately limited by the timing resolution of photon detection (Δt_R). This presents a challenge to networks with heterogeneous nodes or those that rely on spectral multiplexing; for example, a π phase uncertainty at a frequency difference of just 10 GHz corresponds to $\Delta t_R = 50$ ps. Although detector jitters have reached few-picosecond levels and continue to improve [10], alternative Bell state analyzers (BSAs) that automatically erase spectral distinguishability would offer significant value, eliminating the need for feedforward phase correction techniques that introduce latency and increase complexity.

In this work, we demonstrate a BSA that leverages frequency beamsplitter concepts [11–16] to operate on frequency mismatch directly. Through the use of interleaved Hadamard gates in a quantum frequency processor, we realize unambiguous measurement of two frequency-bin-encoded Bell states with a fidelity of 98%. Our design can be extended to Bell state measurements of qubits encoded in other degrees of freedom as well—e.g., where frequency is used for multiplexing only—such as time-bin or polarization qubits that otherwise would not interfere. Overall, our demonstration makes it possible to break the trade-off between spectral distinguishability and remote entanglement fidelity, representing an important step toward the long-term vision of a quantum internet that is compatible with both heterogeneous nodes and dense spectral multiplexing.

Figure 1(a) highlights the challenges faced in implementing conventional spatial BSAs in wavelength-multiplexed fiber-optic networks. On the one hand, photons with identical carrier frequencies are optimal for Bell state measurements, yet the selective adding and dropping of separate photons with identical spectra is incompatible with wavelength multiplexers, creating bandwidth contention issues. On the other hand, spectrally distinct photons can be readily multiplexed but require fine temporal resolution in the BSA to mitigate the distinguishability otherwise present with frequency mismatch. Our proposed solution is outlined in Fig. 1(b). Here, all photons enter the network on a distinct available wavelength channel; to implement a BSA, two photons are spectrally isolated and measured directly with a "frequency-mismatch-erasing" operation. In our case we leverage the flexibility of a quantum frequency processor (QFP), which is capable of synthesizing arbitrary unitary transformations in discrete frequency bins [17,18]. Experimentally, we focus on a three-element QFP as pictured in Fig. 1(c), consisting of a pulse shaper sandwiched between two electro-optic phase modulators (EOMs). The EOMs

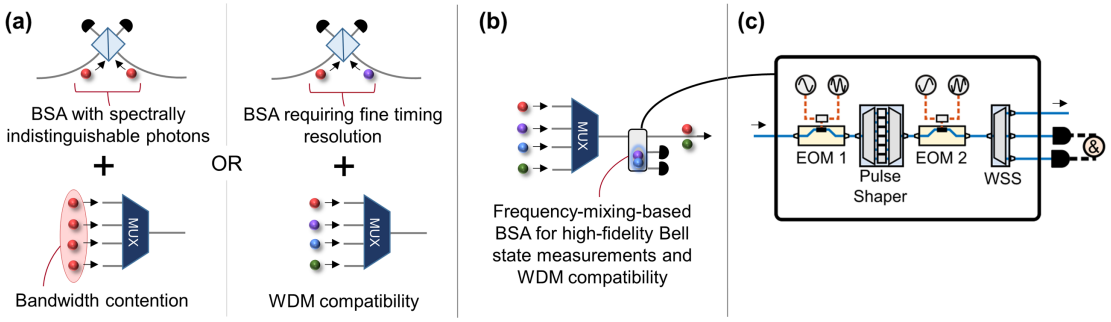

Fig. 1. (a) Conventional BSAs are incompatible with wavelength-division multiplexed networks, which support wavelength-selective aggregation and routing with multiplexing hardware (MUX). (b) A frequency-mixing-based solution, in which all photons carry distinct frequencies, and Bell state measurements erase frequency mismatch directly. (c) Configuration proposed and analyzed, based on a three-element QFP driven with dual-tone electro-optic modulation.

are driven by a superposition of two microwave tones, equal to the fundamental frequency-bin spacing and its second harmonic. Such a two-tone setup matches the most expressive QFP hitherto demonstrated (in terms of the number of parameters available for design) which was previously explored to realize a frequency-bin tritter—a three-mode generalizaton of the beam splitter [14]. The importance of eliminating frequency mismatch applies to photons carrying quantum information in any degree of freedom. However, in light of the synergies of frequency encoding with both matter-based qubits that leverage multiple energy levels and fiber-optic networks built on wavelength multiplexing, we design our BSA for frequency-bin qubits specifically. Suppose that the photons to be measured exist in a superposition of frequency bins $\{A_0, A_1\}$ (qubit A) and $\{B_0, B_1\}$ (qubit B) selected from a predefined grid spaced in multiples of $\Delta\omega$. Following the conventional polarization-qubit BSA [19,20], the desired transformation should mix the logical-0 modes of both photons (A_0 and B_0) according to a 50:50 beamsplitter, i.e., Hadamard operation; the logical-1 modes (A_1 and B_1) should also be mixed according to a Hadamard gate. Two of the four Bell states—expressed in the Fock basis as $|\Psi^{\pm}\rangle \propto |1_{A_0} 1_{B_1}\rangle \pm |1_{A_1} 1_{B_0}\rangle$ in this design—produce unique coincidence patterns in the output modes and can be unambiguously identified.

Significantly, the design of such a BSA in the frequency domain introduces nuances regarding logical encoding definitions that are typically of minimal concern in the path or polarization paradigms. For example, due to the ready availability of inexpensive, passive components that can transform from any polarization basis to another, a $|\Psi^{\pm}\rangle$-state BSA can be adjusted to respond to a different pair of Bell states simply by incorporating an appropriate sequence of wave plates. Analogous basis transformations are attainable within frequency-bin encoding as well, yet because they require additional EOMs and pulse shapers to realize, certain logical encodings may prove much more efficient to implement than others, in terms of total QFP resources (number of components and bandwidth). Accordingly, judicious placement of frequency modes can prove critical in the synthesis of multiphoton QFP gates, as evidenced by previous controlled-unitary designs [17,21] that attain high fidelities with appreciably fewer QFP elements than the $\mathcal{O}(N)$ worst-case scaling for an N-mode unitary [17].

In order to connect our experiment to situations typical for biphoton frequency combs, we assume a fixed frequency grid in our initial design. Specifically, consider as resources four adjacent modes centered at the frequencies $\{\omega_{-1}, \omega_0, \omega_1, \omega_2\}$, where $\omega_n = \omega_0 + n\Delta\omega$. The frequency-bin transformation corresponding to a $|\Psi^{\pm}\rangle$-state BSA depends on whether the qubits are placed in either (i) interleaved or (ii) adjacent fashions. In encoding (i), we can define the logical modes as $(A_0, A_1) = (\omega_{-1}, \omega_1)$ and $(B_0, B_1) = (\omega_0, \omega_2)$; for encoding (ii), the adjacent qubit definitions $(A_0, A_1) = (\omega_{-1}, \omega_0)$ and $(B_0, B_1) = (\omega_1, \omega_2)$ apply. Then, the required unitaries operating on the annihilation operators associated with each bin $(\hat{a}_{-1}, \hat{a}_0, \hat{a}_1, \hat{a}_2)^T$ are

$$U^{(\mathrm{i})} = \frac{1}{\sqrt{2}}\begin{pmatrix} 1 & 1 & 0 & 0 \\ 1 & -1 & 0 & 0 \\ 0 & 0 & 1 & 1 \\ 0 & 0 & 1 & -1 \end{pmatrix}; \quad U^{(\mathrm{ii})} = \frac{1}{\sqrt{2}}\begin{pmatrix} 1 & 0 & 1 & 0 \\ 0 & 1 & 0 & 1 \\ 1 & 0 & -1 & 0 \\ 0 & 1 & 0 & -1 \end{pmatrix}. \tag{1}$$

We note that while Ref. [15] also considered parallel frequency beam splitters, these were separated by a guard band and operated on two photons independently, whereas the BSA here must intentionally mix two photons. In this way, the straightforward parallelization in Ref. [15] cannot be applied, making the design requirements for the frequency BSA significantly more stringent. To compare the feasibility of each proposed encoding, we determine the optimal pulse shaper and EOM settings for the QFP in Fig. 1(c) using particle swarm optimization (PSO) [22]. Defining W as the actual 4×4 mode transformation for a specific QFP configuration, PSO attempts to minimize the cost function $C = \mathcal{P}_W \log_{10}(1 - \mathcal{F}_W)$, where the fidelity $\mathcal{F}_W = |\mathrm{Tr}(W^\dagger U)|^2/(16\mathcal{P}_W)$ and success probability $\mathcal{P}_W = \mathrm{Tr}(W^\dagger W)/4$ are defined in the modal sense—i.e., with respect to the desired mode unitary $U \in \{U^{(\mathrm{i})}, U^{(\mathrm{ii})}\}$—as distinct from the BSA fidelity $\mathcal{F}_{\pm}$ defined later.

The optimal solutions for each encoding appear in Fig. 2, which show the specific EOM modulation patterns plotted over the fundamental period $T = \frac{2\pi}{\Delta\omega}$, pulse shaper phase shifts, and complete transformation matrix W. We allow the pulse shaper to modulate up to 32 frequency bins to account for any spreading outside of the computational space induced by the first EOM. Phasor notation is used for plotting the complex matrix elements: the color signifies the amplitude, with the scale bar normalized to the maximum value in each matrix (0.6831 for $U^{(\mathrm{i})}$ and 0.6978 for $U^{(\mathrm{ii})}$), and the radial line marks out the phase. The QFP can realize both unitaries with high fidelity ($\mathcal{F}_W = 1 - 10^{-6}$ for both) and success probability ($\mathcal{P}_W = 0.9310$ for $U^{(\mathrm{i})}$ and $\mathcal{P}_W = 0.9739$ for $U^{(\mathrm{ii})}$). Nevertheless, the adjacent qubit encoding [Fig. 2(b)] entails a significantly smaller maximum temporal phase deviation (0.8283 rad) compared to the interleaved encoding (4.426 rad)

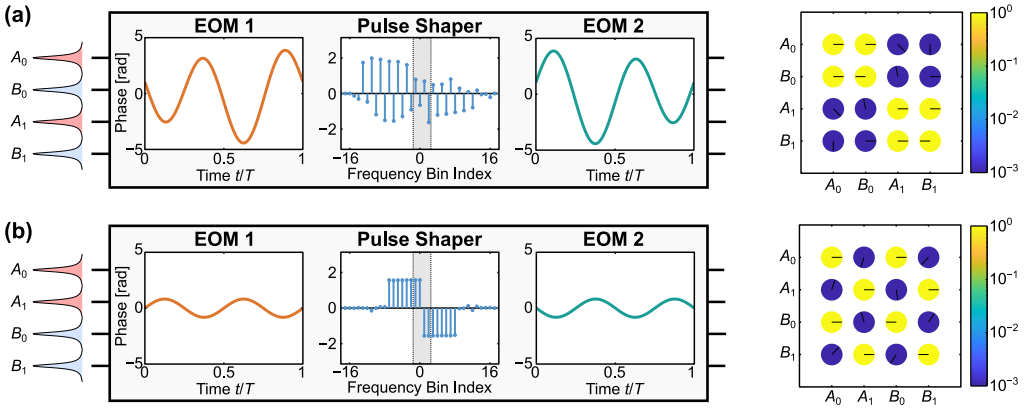

Fig. 2. Optimal QFP designs for frequency-bin BSA. (a) Interleaved qubits [encoding (i)]. (b) Adjacent qubits [encoding (ii)]. The temporal and phase modulation patterns correspond to each component in the setup of Fig. 1(c); the four computational modes are denoted with gray shading in the pulse shaper plot. The mode transformation matrices are depicted to the right, where the amplitude (phase) of each element is represented by the color (radial line) of the corresponding circle.

and consists entirely of a pure sine wave at the harmonic frequency $2\Delta\omega$. In fact, this solution is precisely that of two frequency-bin beam splitters following the design of Refs. [14,23], each operated at twice the fundamental spacing and shifted by one bin with respect to the other. On the other hand, the solution of Fig. 2(a) is not clearly related to previous frequency beam splitters, which makes sense: the fidelity of two parallel beam splitters in Ref. [14] was found to drop rapidly with guardband separations less than two bins, so a significantly different design is required to reduce cross talk for the contiguous beam splitters in $U^{(\mathrm{i})}$.

Given the greater simplicity of the QFP solution for encoding (ii), we select it for experimental implementation. The setup for state preparation, QFP operation, and photon detection mirror configurations from previous work [15,21], but with noteworthy technical improvements including a ridge waveguide biphoton source, narrower bin spacing, and higher-bandwidth microwave components to reach 40 GHz. Taking a separation of $\Delta\omega/2\pi = 20$ GHz and $\omega_0/2\pi \approx 192.2$ THz, we implement the QFP solution in Fig. 2(b). Figure 3(a) plots measured input/output spectra for classical single-frequency inputs, highlighting independent and balanced mixing between bins $(A_0,\ B_0) = (\omega_{-1},\ \omega_1)$ and between $(A_1,\ B_1) = (\omega_0,\ \omega_2)$; the fraction of the output flux in the four-mode computational space is 0.973 on average, in excellent agreement with the theoretical unitary success probability $\mathcal{P}_W = 0.9739$. Our Bell states for testing are generated through type-0 parametric downconversion in a periodically poled lithium niobate ridge waveguide that is pumped by a continuous-wave laser at twice the frequency of the spectral center $\omega_0 + \Delta\omega/2$. We carve out 20 GHz spaced frequency bins using a fiber-pigtailed etalon with an intensity full-width at half-maximum of 0.8 GHz. A subsequent pulse shaper blocks all but the four frequency bins $\{A_0,\ A_1,\ B_0,\ B_1\}$ which ideally produces the state $|\Psi^+\rangle$; by applying a π phase shift onto frequency bin B_0 as well, $|\Psi^-\rangle$ can be produced. (We did not examine the positively correlated $|\Phi^\pm\rangle$ Bell states, which cannot be distinguished in our setup due to the well-known 50% efficiency of vacuum-assisted linear-optical BSAs [24,25].) After traversing the QFP, the output is frequency demultiplexed and routed to two superconducting nanowire single-photon detectors. Coincidence counts for all six detector combinations—A_0A_1, A_0B_0, A_0B_1, A_1B_0, A_1B_1, and B_0B_1—are collected within a 1.5 ns window and integrated for a total of

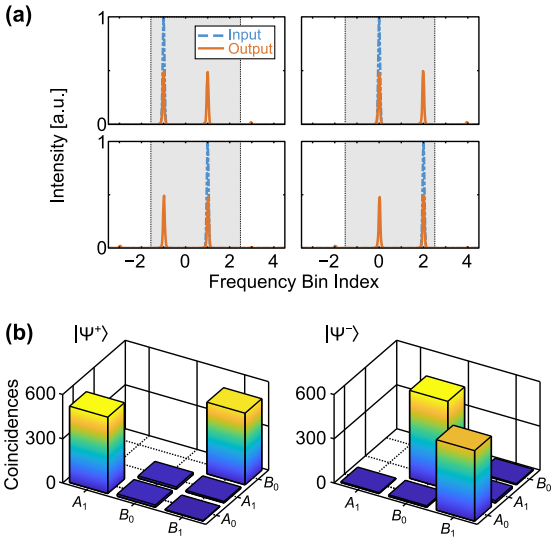

Fig. 3. Experimental results for frequency-bin BSA. (a) QFP outputs when excited by monochromatic classical inputs, obtained from an optical spectrum analyzer. Gray boxes outline the computational modes. (b) Coincidences in all six combinations of output bins when probed by $|\Psi^\pm\rangle$ entangled states.

120 s. Experimental results are presented in Fig. 3(b). For the $|\Psi^+\rangle$ input, coincidences register between the two frequencies corresponding to the modes A_0A_1 or B_0B_1; for $|\Psi^-\rangle$, coincidences are obtained in A_0B_1 or A_1B_0, thereby allowing unambiguous differentiation of $|\Psi^\pm\rangle$ as designed [20]. We calculate the BSA fidelity $\mathcal{F}_\pm = N_C/(N_C + N_I)$ for each input $|\Psi^\pm\rangle$, where N_C and N_I correspond, respectively, to the sum of the two correct measurement results and the sum of the two incorrect results. We find $\mathcal{F}_+ = (98.1 \pm 0.4)\%$ and $\mathcal{F}_- = (98.6 \pm 0.4)\%$, assuming Poissonian error bars and without subtraction of accidentals; if we *do* subtract accidentals, these values increase to $(99.4 \pm 0.3)\%$ and $(99.8 \pm 0.1)\%$, respectively, indicating our raw fidelities are limited primarily by multipair events and dark counts, and not the BSA operation itself.

In this proof-of-principle experiment, we used a continuous-wave pump laser for convenience as temporal correlations within

each pair synchronize photon arrival at the BSA. However, applications in quantum networking will require pulsed operation, both to facilitate synchronization across multiple sites and to erase spectral distinguishability *within* any individual spectral mode. Our BSA design should readily support such clocked inputs and is only limited by the photon bandwidth. For the ∼1 GHz frequency bins in our work, pump pulse rates up to ∼1 GHz are in principle feasible. From a timing perspective, any nonlocal scenario will require photons to arrive at the BSA stabilized to within a fraction of the QFP drive signal period (25 ps at the current 40 GHz modulation frequency). However, our frequency-mixing BSA ensures that photon detectors only need to resolve the temporal spacing between successive pump pulses—a more lenient condition.

Our QFP approach is not the only possible way to synthesize BSAs based on frequency mixing. A single EOM is sufficient to realize a probabilistic frequency-bin beam splitter, whereby photonic energy scattered into adjacent sidebands is lost and not compensated through subsequent stages; this simpler design has been employed in single-photon entanglement swapping protocols [26], as well as frequency-bin Hong–Ou–Mandel interference experiments [27,28], suggesting promise in a complete BSA. A coupled-cavity–based frequency-bin beam splitter [29,30] eliminates the additional sidebands produced by a nonresonant EOM and therefore provides a highly compact, integrated platform for future BSAs. Finally, through appropriate design of classical pump fields and phase-matching conditions, frequency beam splitters based on $\chi^{(2)}$ [12] and $\chi^{(3)}$ [13,16] optical nonlinearities provide opportunities for frequency-bin BSAs bridging large (terahertz and beyond) spectral separations, thus complementing the gigahertz-level spacings ideal for electro-optic designs.

Funding. U.S. Department of Energy, Office of Science (ASCR - Early Career Research Program); Air Force Research Laboratory (FA8750-20-P-1705); National Science Foundation (1747426-DMR, 2034019-ECCS).

Acknowledgment. Preliminary results were presented at IPC 2020 as paper number PD5 and CLEO 2021 as paper number FTu1N.5. We thank AdvR for loaning the PPLN ridge waveguide. A portion of this work was performed at Oak Ridge National Laboratory, operated by UT-Battelle for the U.S. Department of Energy under contract no. DE-AC05-00OR22725.

Disclosures. The authors declare no conflicts of interest.

Data availability. Data available from the authors on request.

[†]These authors contributed equally to this Letter.

REFERENCES

1. S. Wehner, D. Elkouss, and R. Hanson, Science **362**, eaam9288 (2018).
2. L.-M. Duan and H. J. Kimble, Phys. Rev. Lett. **90**, 253601 (2003).
3. B. Zhao, Z.-B. Chen, Y.-A. Chen, J. Schmiedmayer, and J.-W. Pan, Phys. Rev. Lett. **98**, 240502 (2007).
4. N. Sangouard, C. Simon, H. De Riedmatten, and N. Gisin, Rev. Mod. Phys. **83**, 33 (2011).
5. C. H. Bennett, G. Brassard, C. Crépeau, R. Jozsa, A. Peres, and W. K. Wootters, Phys. Rev. Lett. **70**, 1895 (1993).
6. D. Bouwmeester, J.-W. Pan, K. Mattle, M. Eibl, H. Weinfurter, and A. Zeilinger, Nature **390**, 575 (1997).
7. S. Pirandola, J. Eisert, C. Weedbrook, A. Furusawa, and S. L. Braunstein, Nat. Photonics **9**, 641 (2015).
8. T.-M. Zhao, H. Zhang, J. Yang, Z.-R. Sang, X. Jiang, X.-H. Bao, and J.-W. Pan, Phys. Rev. Lett. **112**, 103602 (2014).
9. G. Vittorini, D. Hucul, I. Inlek, C. Crocker, and C. Monroe, Phys. Rev. A **90**, 040302 (2014).
10. I. E. Zadeh, J. Chang, J. W. N. Los, S. Gyger, A. W. Elshaari, S. Steinhauer, S. N. Dorenbos, and V. Zwiller, Appl. Phys. Lett. **118**, 190502 (2021).
11. M. Raymer, S. van Enk, C. McKinstrie, and H. McGuinness, Opt. Commun. **283**, 747 (2010).
12. T. Kobayashi, R. Ikuta, S. Yasui, S. Miki, T. Yamashita, H. Terai, T. Yamamoto, M. Koashi, and N. Imoto, Nat. Photonics **10**, 441 (2016).
13. S. Clemmen, A. Farsi, S. Ramelow, and A. L. Gaeta, Phys. Rev. Lett. **117**, 223601 (2016).
14. H.-H. Lu, J. M. Lukens, N. A. Peters, O. D. Odele, D. E. Leaird, A. M. Weiner, and P. Lougovski, Phys. Rev. Lett. **120**, 030502 (2018).
15. H.-H. Lu, J. M. Lukens, N. A. Peters, B. P. Williams, A. M. Weiner, and P. Lougovski, Optica **5**, 1455 (2018).
16. C. Joshi, A. Farsi, A. Dutt, B. Y. Kim, X. Ji, Y. Zhao, A. M. Bishop, M. Lipson, and A. L. Gaeta, Phys. Rev. Lett. **124**, 143601 (2020).
17. J. M. Lukens and P. Lougovski, Optica **4**, 8 (2017).
18. H.-H. Lu, A. M. Weiner, P. Lougovski, and J. M. Lukens, IEEE Photon. Technol. Lett. **31**, 1858 (2019).
19. S. L. Braunstein and A. Mann, Phys. Rev. A **51**, R1727 (1995).
20. K. Mattle, H. Weinfurter, P. G. Kwiat, and A. Zeilinger, Phys. Rev. Lett. **76**, 4656 (1996).
21. H.-H. Lu, J. M. Lukens, B. P. Williams, P. Imany, N. A. Peters, A. M. Weiner, and P. Lougovski, npj Quantum Inf. **5**, 24 (2019).
22. J. Kennedy and R. Eberhart, in *International Conference on Neural Networks* (1995), Vol. **4**, p. 1942.
23. H.-H. Lu, N. Klco, J. M. Lukens, T. D. Morris, A. Bansal, A. Ekström, G. Hagen, T. Papenbrock, A. M. Weiner, M. J. Savage, and P. Lougovski, Phys. Rev. A **100**, 012320 (2019).
24. N. Lütkenhaus, J. Calsamiglia, and K.-A. Suominen, Phys. Rev. A **59**, 3295 (1999).
25. J. Calsamiglia and N. Lütkenhaus, Appl. Phys. B **72**, 67 (2001).
26. S.-Y. Lan, S. D. Jenkins, T. Chanelière, D. N. Matsukevich, C. J. Campbell, R. Zhao, T. A. B. Kennedy, and A. Kuzmich, Phys. Rev. Lett. **98**, 123602 (2007).
27. P. Imany, O. D. Odele, M. S. Alshaykh, H.-H. Lu, D. E. Leaird, and A. M. Weiner, Opt. Lett. **43**, 2760 (2018).
28. A. Khodadad Kashi and M. Kues, Laser Photon. Rev. **15**, 2000464 (2021).
29. M. Zhang, C. Wang, Y. Hu, A. Shams-Ansari, T. Ren, S. Fan, and M. Lončar, Nat. Photonics **13**, 36 (2019).
30. Y. Hu, M. Yu, D. Zhu, N. Sinclair, A. Shams-Ansari, L. Shao, J. Holzgrafe, E. Puma, M. Zhang, and M. Loncar, Nature **599**, 587 (2021).

73.102.246.144 (ts 2022-04-19 16:16:25)